International Scholarly Research Network
ISRN Materials Science
Volume 2012, Article ID 804763, 9 pages
doi:10.5402/2012/804763

Research Article

Time-Dependent Oxidative Capacities of La_2O_3, Lu_2O_3, CeO_2, and Bi_2O_3 Materials Interacting with Air-CO or Air-CH_4 Flows

Bahcine Bakiz,[1] Lamia Bourja,[1,2] Abdeljalil Benlhachemi,[2] Frederic Guinneton,[1] Sylvie Villain,[1] Mohamed Ezahri,[2] and Jean-Raymond Gavarri[1]

[1] *Institut Matériaux Microélectronique et Nanosciences de Provence (IM2NP), UMR CNRS 6242, Université du Sud Toulon-Var, BP 20132, 83957 La Garde Cedex, France*
[2] *Laboratoire Matériaux et Environnement (LME), Faculté des Sciences, Université Ibn Zohr, BP 32/S, Cité Dakhla, Agadir 8106, Morocco*

Correspondence should be addressed to Jean-Raymond Gavarri, gavarri.jr@univ-tln.fr

Received 22 August 2012; Accepted 29 September 2012

Academic Editors: I. Imae, G. C. Mather, and R. A. Varin

Using Fourier transform infrared (FTIR) spectroscopy analyses, we have studied the oxidation processes of methane or carbon monoxide in air-CH_4 or air-CO flows interacting with polycrystalline catalytic oxides, as a function of temperature *(T)* and time *(t)*. The gas flows crossed through La_2O_3, Lu_2O_3, CeO_2, or Bi_2O_3 porous walls with constant composition and rate. The oxidation capacities of materials were determined from the intensities $I(t, T)$ of CO_2 vibrational bands resulting from the total oxidation of CH_4 or CO into CO_2. To interpret the time-dependent variations of these intensities, we have applied a model derived from Johnson-Mehl-Avrami approaches. This simple approach delivers pertinent parameters describing time-dependent oxidation rates.

1. Introduction

In the general framework of catalytic gas sensing or depolluting microsystems development, we study the time-dependent oxidation capacities of polycrystalline materials interacting with air-CO or air-CH_4 gas flows. The main objective is to convert toxic CO or undesired CH_4 gases into CO_2 gas. To follow the reaction processes, we make use of Fourier transform infrared spectroscopy and determine the time- (t) and temperature- (T) dependent intensities $I(t, T)$ of CO_2 vibrational bands resulting from the oxidation processes of CH_4 or CO in air-CH_4 or air-CO gas flows. In this study, we determine the catalytic efficiencies of La_2O_3, Lu_2O_3, CeO_2, and Bi_2O_3 polycrystalline oxides as a function of reaction time, at various temperatures: the air-CH_4 or air-CO flows cross through porous polycrystalline walls of these rare earth-based oxides and a system based on the Bi_2O_3 phase [1].

Rare earth oxides are well known for the similarity of their chemical and physical properties, in relation with the electronic structures (4f-5d-6s) of rare earth cations. Despite this similarity, these oxides generally present diversified physical and chemical properties allowing their use in many applications. The cerium oxide (ceria) has been extensively studied as a catalyst [2–5] or semiconducting material [6–8]. The catalytic properties of ceria have been ascribed to the capacity of cerium to change its valence from Ce^{4+} to Ce^{3+} and thus to oxidize or reduce gases. In the case of lanthanum oxide (lantana), catalytic behaviours have been studied in the past [9]. This oxide is used in the conversion of CH_4 into syngas (H_2 + CO) [10]. However, very few studies on the reactivity of lutetium oxide (lutetia) in presence of gases are available in the literature: this oxide is mainly involved in optical, luminescence applications [11–14]. In 1976, the catalytic oxidation of butane was studied over a series of lanthanide oxides in order to investigate the effect of the electronic configuration on the catalytic activity [15]. The authors showed that lanthanum oxide was one of the least active catalysts; cerium oxide was the most active one, and the activity decreased with an increase in the atomic

number from cerium to gadolinium. They also observed that the activity of terbium oxide was the second highest, and again the activity decreased from terbium to lutetium. In other terms, for the authors, lutetia should have the weakest activity in the case of oxidation of butane.

In the case of our previous studies on the system Bi_2O_3-CeO_2 [1], we clearly observed a high catalytic activity of the bismuth oxide interacting with air-CO gas flows and a poor activity of this oxide in presence of air-CH_4 gas flows.

In these experimental studies [1], the evolution *versus* time of oxidation capacities $I(t, T)$ (CH_4 or CO being converted into CO_2) presents a common behavior, characterized by at least three periods: initiating, intermediate, and stabilization periods. Some samples present abnormal maxima of $I(t, T)$ in the intermediate period of reaction. Such behaviors might be conditioned by the nature of grain surfaces in the materials.

In the present study, we try to interpret the time-dependent evolutions of the FTIR intensities $I(t, T)$ using elemental Avrami models [16–18]. The modeling approach is applied to La_2O_3, CeO_2, Lu_2O_3, and Bi_2O_3 phases.

2. Experimental Section

2.1. Samples. The various samples were synthesized via specific routes previously described by us [1, 19–22] and based on wet chemistry processes involving nitrate-based solutions. The ceria phase was elaborated in nanocrystalline form at 200°C. The La_2O_3 and Lu_2O_3 were obtained after final thermal treatment at 750°C. The Bi_2O_3 phase was obtained after thermal treatment at 600°C during 4 hours. Each polycrystalline phase was clearly identified using classical X-ray diffraction from D5000 Bruker equipment in θ–2θ configuration. Brunauer-Emmett-Teller (BET) [23] analyses were carried out to determine the sample-specific surface areas noted as A_{BET} in m^2/g. This method delivers the effective surface exposed to gas adsorption. In the case of absence of agglomerations, the A_{BET} values can be related to individual grain dimensions. The A_{BET} values were found to be 11.5 m^2/g for La_2O_3, 82.0 m^2/g for CeO_2, 5.0 m^2/g for Lu_2O_3, and 2.0 m^2/g for Bi_2O_3.

2.2. FTIR Spectroscopy and Reactivity Analyses. The rare earth or bismuth-based materials were exposed to air-CH_4 and air-CO gas flows in a homemade cylindrical reaction cell (see Figure 1). The transformation of CH_4 or CO into CO_2 was analyzed by Fourier transform infrared (FTIR) spectroscopy, using a FTIR Unicam-Mattson-Bruker spectrometer. The gases pass through a polycrystalline porous walls constituted of the various phases. The polycrystalline walls are fixed between two porous separators. A constant mass of $m_0 = 0.1$ g was used in each experiment.

All experimental details have been extensively described in previous works. The conversion reactions are analyzed from the infrared absorption band intensities of CO_2

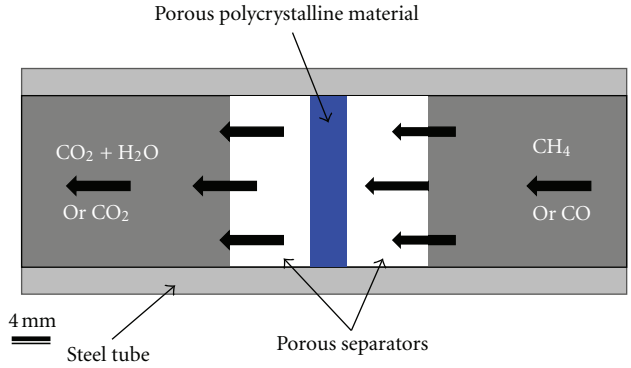

Figure 1: Catalytic reactor.

(doublet at 2340–2360 cm^{-1}), resulting from one of the overall reactions:

$$CH_4 + 2O_2 \longrightarrow CO_2 + 2H_2O \quad (1)$$

$$CO + \frac{1}{2}O_2 \longrightarrow CO_2 \quad (1)'$$

The conversion intensity $I(t, T)$ was determined from the measurements of CO_2 absorption bands, at a certain time t of the gas/solid interaction. Each vibrational spectrum was recorded over a period of $\Delta t = 10$ s with intervals of 30 s between two spectra. The total exposure time was two hours. For a given total time t of reaction and a given temperature T_{react}, the intensity $I(t, T)$ was assumed to be proportional to the amount of CO_2 molecules formed during the time Δt of FTIR record. All experiments were characterized by a first initiating regime in which the CO_2 intensities increase upto a maximal value after a time of about 10–15 minutes.

Figures 2(a) and 2(b) represent typical FTIR spectra associated with conversions of CH_4 and CO after solid gas interactions. The CO_2 FTIR band intensity increases as the CH_4 or CO band intensities decrease.

To compare the various reactivities, we have normalized the curves $I(t, T)$ using the specific surfaces A_{BET} by calculating the values $I^*(t, T) = I(t, T)/A_{BET}$. It should be noted that, in our experiments, the temperature ranges were limited to 275°C for air-CO flows and 525°C for air-CH_4 flows in order to avoid direct oxidation of CO or CH_4 by oxygen (this direct oxidation was tested in our experimental device in the absence of active sample).

3. Modeling Approaches

In our previous work [24], we proposed a semiempirical model based on typical catalytic steps summarized as follows:

(i) surface adsorption of gas and O_2 (air) on the surface of the solid;

(ii) surface reaction $CH_4 + 2O_2 \rightarrow CO_2 + 2H_2O$ or CO + $O_2 \rightarrow CO_2$, with reduction of catalyst surface, followed by CO_2 desorption;

(iii) regeneration of the solid (with oxidation of surfaces) due to adsorbed oxygen from the air;

(iv) desorption of gases.

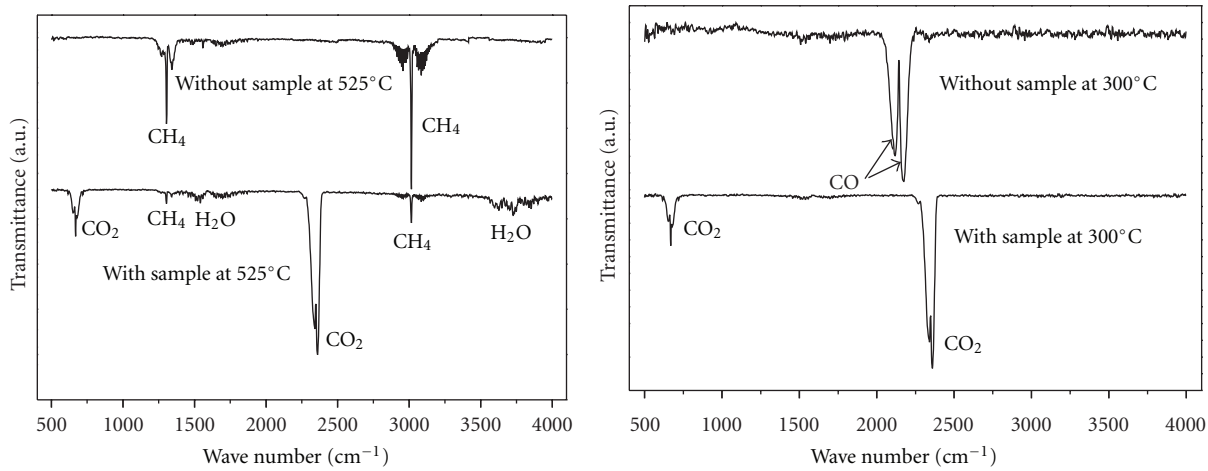

Figure 2: FTIR spectroscopy of emitted gases. Transmittances without any catalytic sample and in presence of a catalyst Lu_2O_3: (a) CH_4 converted into CO_2 and H_2O and (b) CO converted into CO_2.

It should be important to note that, in the present experiments, the gas flows cross through polycrystalline porous walls of materials, with a fixed speed and a fixed gas composition: in these circumstances, the gas-solid interactions result from a complex equilibrium involving four distinct kinetics of adsorption, desorption, degradation, and regeneration of active sites. In our model, we have assumed that the desorption steps of final gases (CO_2) might be described by surface reaction laws.

The intermediate surface reactions between adsorbed molecules and active sites might be described as follows.

(i) Oxidation step of adsorbed molecules from mobile surface oxygen O^* of one active site S_{red}-O^*, delivering one reduced site "S_{red}":

$$\begin{aligned}(CH_4)_{ads} + 4S_{red}\text{-}O^* &\longrightarrow (CH_4)_{ads} + 4S_{red} + 4O^* \\ &\longrightarrow CO_2 + 4S_{red} + 2H_2O\end{aligned} \tag{2}$$

or

$$\begin{aligned}(CO)_{ads} + S_{red}\text{-}O^* &\longrightarrow (CO)_{ads} + S_{red} + O^* \\ &\longrightarrow CO_2 + S_{red}\end{aligned} \tag{3}$$

(i) Formation of mobile oxygen species O^* from adsorbed dioxygen from air: $(O_2)_{ads} \rightarrow 2O^*$.

(ii) Regeneration (oxidation) of reduced sites "S_{red}":

$$4S_{red} + 4O^* \longrightarrow 4S_{red}\text{-}O^* \tag{4}$$

or

$$S_{red} + O^* \longrightarrow S_{red}\text{-}O^* \tag{5}$$

The general expression delivering the CO_2 vibrational band intensity is assumed to result from sites delivering oxygen S_{red}-O^* and sites regenerated from oxygen from air S_{red}:

$$\frac{d[CO_2]}{dt} = I(t,T) = A(t,T)[D(t,T) + R(t,T)]. \tag{6}$$

In this expression, the symbol $[CO_2]$ designates the total amount of CO_2 molecules formed after a reaction time 0074. The derivative $d[CO_2]/dt = \Delta[CO_2]/\Delta t$ is proportional to the instantaneous amount $\Delta[CO_2]$ recorded at time t, during the period Δt. The term $A(t,T)$ describes the adsorption of gases on the solid surfaces, $D(t,T)$ describes the reaction between oxidative active sites and reducing gas molecules, and $R(t,T)$ describes the site regeneration due to oxygen from air adsorbed at the solid surface. Each A, D, R term was previously expressed using three distinct Avrami's approaches. The final general expression adapted to the normalized data $I^* = I/A_{BET}$ was as follows:

$$\begin{aligned}I^*(t,T) = X_0 \cdot [1 - \exp(-K_0 t)] \\ \cdot \{S_1 \cdot \exp(-K_1 t^p) + S_2[1 - \exp(-K_2 t^q)]\}.\end{aligned} \tag{7}$$

In this expression, the parameter X_0 is proportional to the composition of the air-gas flow. This composition (2500 ppm in air) was fixed for all experiments. As the normalized I^* values characterize the instantaneous amounts of CO_2 molecules formed per surface unit of material, the X_0 parameter can act as a scaling factor. The K_0 kinetics factors result from first-order classical adsorption law. The parameters S_1 and S_2 are linked to the initial active sites (oxygen donors) and to the final re-activated sites, respectively, due to oxygen (air) action. The K_1 and K_2 parameters and p, q exponents result from specific Avrami models and are conditioned by the chemical processes of degradation or reconstructive growth. Surface degradation is conditioned by the presence of initial O^* species reacting with adsorbed "gas" molecules in increasing number (because of the constant gas flow).

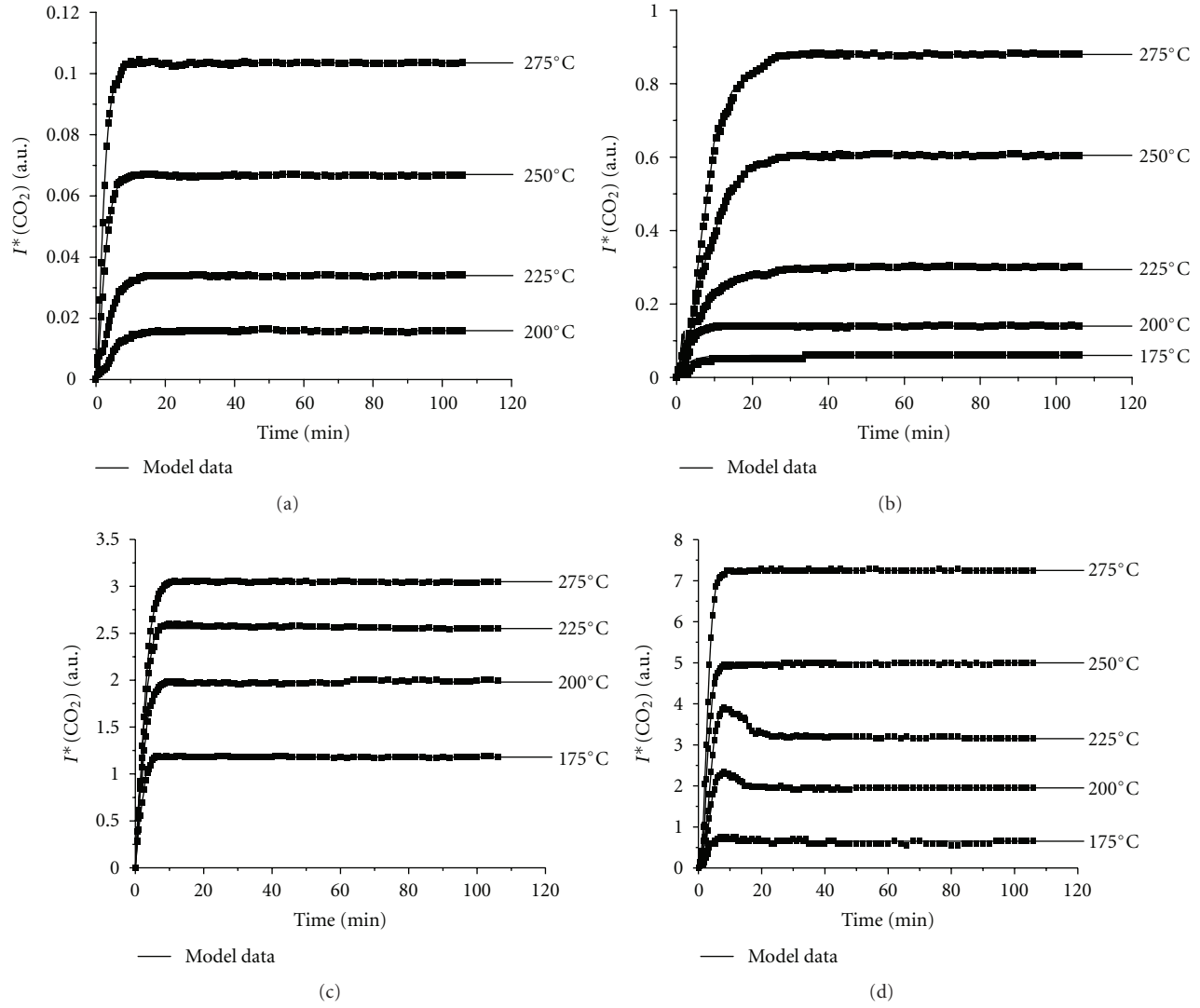

Figure 3: Simulation of CO oxidation efficiencies in the case of air-CO flows (2500 ppm CO) interacting with: (a) CeO_2; (b) La_2O_3; (c) Lu_2O_3; (d) Bi_2O_3 as a function of time and for various temperatures. Experimental data: dotted line; model data: continuous line.

The degradation mechanism requires interaction between one adsorbed molecule "gas" and one active site delivering a free O^* species. This interaction is complex and could be divided into three main steps:

(i) reduction step with formation of one oxygen vacancy and one O^* free oxygen species,

(ii) O^* migration out of the solid,

(iii) reaction between gas (CH_4 or CO) and O^* giving rise to CO_2.

In our calculations, we tried some adjustments of this parameter. Finally, the value $p = 2$ was found to be satisfactory.

Surface regeneration is associated with a first-order reaction between surface molecules $[O^*]^{\text{air}}_{\text{surf}}$ (or oxygen O_2 from air) and the solid. To regenerate active sites, a lot of O^* surface species (from air) are available on the solid surface: no substantial O^* migration is required to interact with one active site. This is the reason why an exponent $q = 1$ might be expected for such a mechanism. We have fixed this value in our calculations.

As X_0 is a scale factor, five pertinent parameters result from our hypotheses. The K_0 constant is the adsorption parameter, the K_1 constant is the kinetics parameter associated with adsorption and reaction with one active site, and the K_2 constant is the corresponding kinetics parameter of oxygen regenerating one deactivated site. The S_1 and S_2 constants are proportional to the initial surface area of active sites and final surface area of reactivated sites, respectively.

Regarding the surface reactions, the active sites subjected to degradation (oxygen loss) can be considered as being regenerated by oxygen from air (oxidation), so the numbers of active and regenerated sites are assumed to be equal. Thus, as a first simplified hypothesis, we could assume that S_1 and

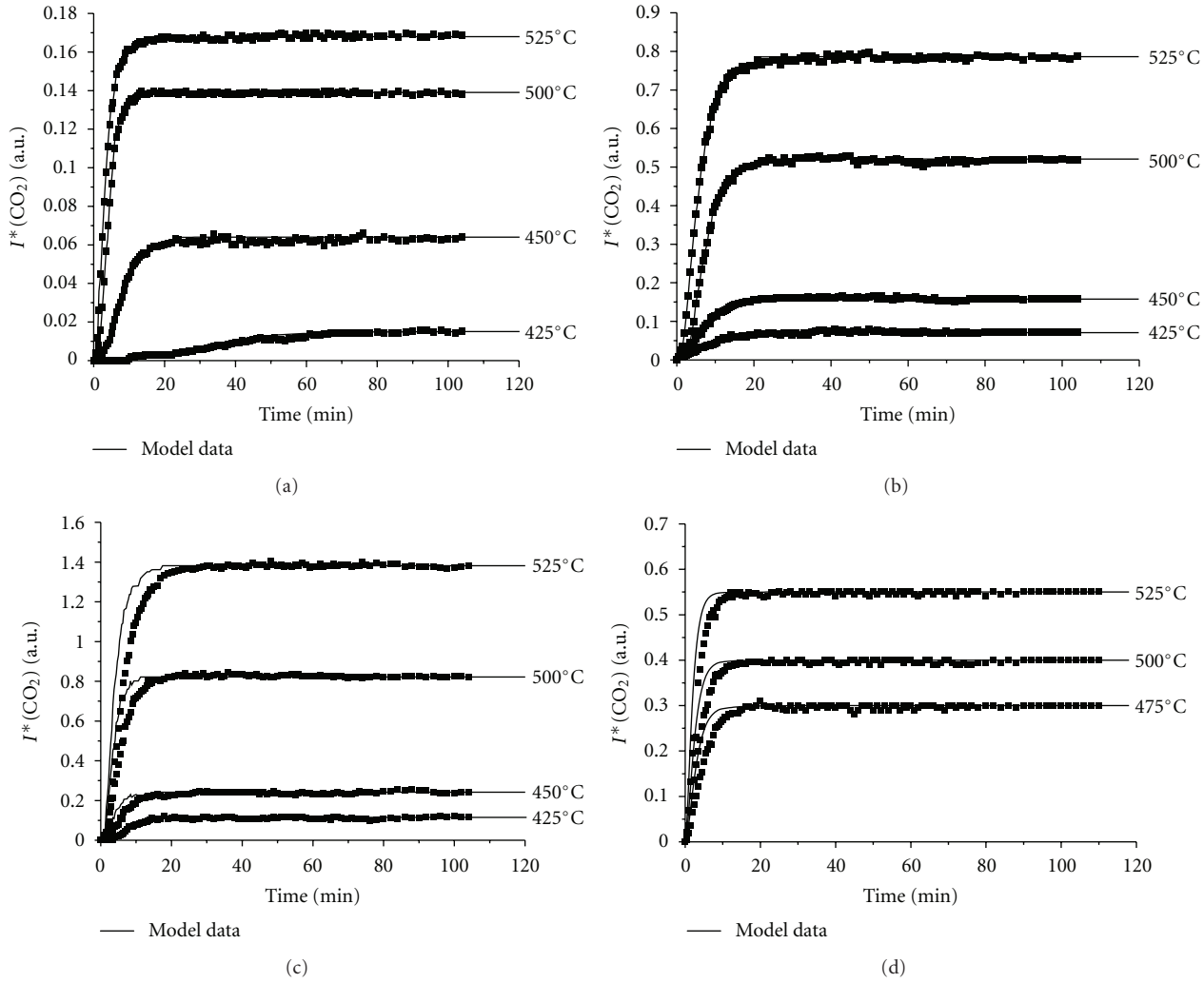

FIGURE 4: Simulation of CH_4 oxidation efficiencies in the case of air-CH_4 flows (2500 ppm CH_4) interacting with: (a) CeO_2; (b) La_2O_3; (c) Lu_2O_3; (d) Bi_2O_3 as a function of time and for various temperatures. Experimental data: dotted line; model data: continuous line.

S_2 should be equal. Therefore, the conversion rate can be expressed as follows:

$$I^*(t,T) = X_0 \cdot S_2 \cdot \left[1 - \exp(-K_0 t)\right] \cdot \left\{\exp\left(-K_1 t^2\right) + \left[1 - \exp(-K_2 t)\right]\right\}. \quad (7)'$$

Apart from the X_0 parameter (scaling factor), each parameter could be dependent on the temperature. The parameters $S_1 = S_2$ depend on the nature of the surface and on the active site densities at a fixed temperature.

For a short experimental time, the expression can be reduced to

$$I^*(t,T) = X_0 \cdot K_0 \cdot S_2 \cdot t. \quad (8)$$

For long experimental time, the expression can be reduced to:

$$I^*_{\max}(t,T) = X_0 \cdot S_2. \quad (9)$$

The maximal values of I^* observed for long reaction times can directly deliver the S_2 term, with X_0 being fixed to an arbitrary value.

4. Results

The first step of calculation consists in assimilating the $I^*_{\max}$ values (constant values reached after a long time of reaction) to $X_0 \cdot S_2$. Then, the various parameters have been adapted to obtain a good fit to the various experimental curves.

In Tables 1 and 2, we have reported the optimized parameters in the cases of air-CO and air-CH_4 gas flows interacting with La_2O_3, CeO_2, Lu_2O_3, and Bi_2O_3.

Figures 3 and 4 give the experimental data and the simulated values of the catalytic efficiencies $I(CO_2)$ of the $(1-x)CeO_2$-$x/2Bi_2O_3 (0 \le x \le 1)$ phases, respectively, interacting with air-CO and air-CH_4 flows (2500 ppm CO or CH_4 in air).

Figures 5(a) and 5(b) compare the $S_2 = S_1$ parameters as a function of temperatures in the case of air-CO and air-CH_4

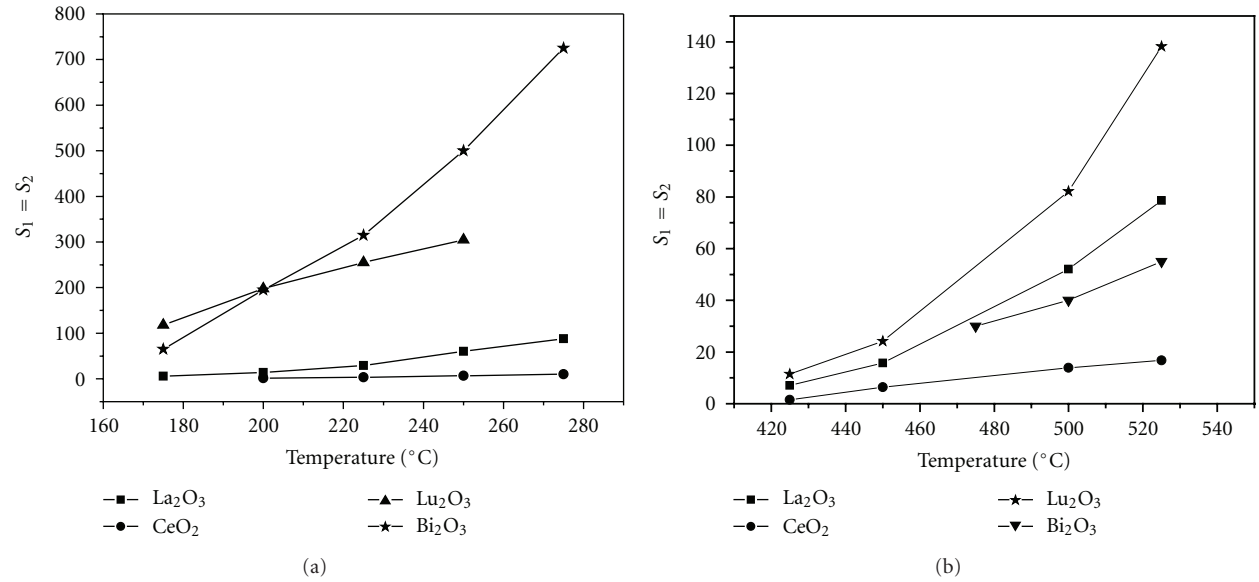

Figure 5: (a) Evolution of $S_1 = S_2$ parameter as a function of temperature in the case of air-CO flows interacting with La_2O_3, CeO_2, Lu_2O_3, and Bi_2O_3. (b) Evolution of $S_1 = S_2$ parameter as a function of temperature in the case of air-CH_4 flows interacting with La_2O_3, CeO_2, Lu_2O_3, and Bi_2O_3.

Table 1: Simulation parameters for solids interacting with air-CO gas flows at various temperatures.

La_2O_3, CeO_2, Lu_2O_3, and Bi_2O_3 interacting with air-CO gas flows					
			La_2O_3		
T °C	K_0	K_1	K_2	S_1	S_2
175	1.8	100	0.34	6	6
200	1.7	500	0.38	14	14
225	0.8	600	0.35	29.2	29.2
250	0.34	850	0.45	60.5	60.5
275	0.31	980	0.57	88	88
			CeO_2		
T °C	K_0	K_1	K_2	S_1	S_2
200	0.27	0.72	0.25	1.6	1.6
225	0.35	0.85	0.35	3.4	3.4
250	0.5	3	0.61	6.7	6.7
275	0.6	4	0.64	10.35	10.35
			Lu_2O_3		
T °C	K_0	K_1	K_2	S_1	S_2
175	2.2	180	2.1	118	118
200	1.83	220	1.84	198	198
225	1.7	250	1.8	255	255
250	1.5	300	1.4	305	305
			Bi_2O_3		
T °C	K_0	K_1	K_2	S_1	S_2
175	1.5	2	1.2	65	65
200	0.47	0.23	1	195	195
225	0.4	0.187	1.2	315	315
250	1.2	3	1.8	500	500
275	1.2	10	2	725	725

Table 2: Simulation parameters for solids interacting with air-CH_4 gas flows at various temperatures.

La_2O_3, CeO_2, Lu_2O_3, and Bi_2O_3 interacting with air-CH_4 gas flows					
			La_2O_3		
T °C	K_0	K_1	K_2	S_1	S_2
425	0.35	1	0.32	7.1	7.1
450	0.36	22	0.5	15.76	15.76
500	0.4	90	0.5	52.1	52.1
525	0.5	100	0.6	78.6	78.6
			CeO_2		
T °C	K_0	K_1	K_2	S_1	S_2
425	0.06	0.8	0.1	1.52	1.52
450	0.34	10	0.46	6.4	6.4
500	0.9	12	0.85	13.9	13.9
525	0.2	15	0.68	16.8	16.8
			Lu_2O_3		
T °C	K_0	K_1	K_2	S_1	S_2
425	0.25	3	0.85	11.49	11.49
450	0.36	12	0.7	24.16	24.16
500	0.55	16	0.6	82.17	82.17
525	0.58	20	0.4	138.2	138.2
			Bi_2O_3		
T °C	K_0	K_1	K_2	S_1	S_2
475	0.26	4	0.33	30	30
500	0.32	7	0.38	40	40
525	0.40	10	0.50	55	55

gases. It should be noted that the calculated curves (Figures 3 and 4) $I^*(t, T)$ fit well the experimental $I^*_{\text{exp}}(t, T)$ data in the initiating periods of catalytic process.

The three K_0, K_1, and K_2 parameters vary with temperature (Tables 1 and 2): they are associated with the adsorption, degradation, and regeneration mechanisms. The S_2 parameter ($S_1 = S_2$) increases with temperature: it is characteristic of the surface of each solid, at specific temperatures and under partial pressures of oxygen from air.

In the case of abnormal behaviors observed during the initiating period, it has been possible to simulate such undulations or maxima. The K_1 parameter is strongly coupled to the K_0 one. It plays a very important role in the short time reactions.

5. Discussion

In the case of air-CO flow interacting with the present oxides, the S_2 (and $S_1 = S_2$) parameters are characteristic of long time behaviors (after initiating period) for all samples and each temperature. Their values directly depend on the choice of unique scale factor X_0, identical in each experiment. They systematically increase with temperature, and their activation energies can be representative of thermal equilibrium at the solid surfaces. The highest values of S_2 regeneration parameters (Tables 1 and 2) are observed for Bi_2O_3 and Lu_2O_3.

The K_0 parameters (Tables 1 and 2) characterize the progressive adsorption of gases and behave diversely as temperature increases. In the case of ceria interacting with air-CO gas, we observe small increasing values; in the case of La_2O_3, they strongly decrease; in the case of Lu_2O_3, they slowly decrease. Finally, in the case of Bi_2O_3, the K_0 values irregularly vary.

The K_1 parameters are correlated with the K_0 parameters, and they play an important role in the initiating and intermediate periods, before the $I_{\max}$ values have been reached. They allow good fitting of undulations observed on several curves (for intermediate time) even if this observation is not systematic. These K_1 parameters are relatively weak in the case of CeO_2 and Bi_2O_3. They have large values in the case of La_2O_3 and Lu_2O_3. This suggests different degradation processes associated with reduction of the solid surfaces. The K_2 parameters characterize the oxidation capacity of the solid surfaces due to oxygen from air. They present two types of similar values, firstly in the case of CeO_2 and Bi_2O_3, and secondly in the case of Lu_2O_3 and Bi_2O_3.

In the case of air-CH_4 flow interacting with the present oxides, all calculated I^* curves fit well the experimental I^* data. The K_0 and K_1 parameters increase with temperature. The $S_2 = S_1$ parameters all increase with temperature. The highest values are observed for Lu_2O_3 sample. These evolutions of parameters are probably conditioned by the specific high stability of methane in presence of oxygen and by a complex decomposition of CH_4 giving rise to two molecules CO_2 and H_2O.

To better interpret the abnormal evolutions observed in the case of Bi_2O_3 oxide (Figure 3(d)), with a maximum of $I(t, T)$ during the intermediate period, at 200 and 225°C, it is possible to invoke the presence of oxygen, carbonate, or hydroxide species, initially adsorbed on grain surfaces of solids, and favor additional oxidation of CO. Such adsorbed species are generally eliminated between 150 and 250°C. After thermal elimination of these surface species (presently for $T > 175$°C), the oxidation process is governed firstly by the oxygen molecules present in gas flows and then by oxygen species delivered by the solids. In the case of methane, as oxidation occurs above 400°C and desorption of species occurs below 400°C, the elimination of such surface species cannot be observed.

6. Conclusions

The Johnson- Avrami Mehl models allowed us to determine pertinent parameters characteristic of the porous media and of the two kinds of gas-solid interactions involving methane or carbon monoxide gases. The different time-dependent oxidation processes characterized by at least three steps have been well described from these parameters: (i) the initiating period is governed by the K_0 parameter, (ii) the intermediate period is governed by both K_0 and K_1 parameters, and (iii) the stabilization period is governed by the S_2 parameter. This last parameter represents the number of active sites at the internal solid surfaces and conditions the catalytic efficiencies for long reaction time: it is directly related to regeneration of solid surfaces via oxygen from air. The K_0 and K_1 parameters represent successively the adsorption kinetics of CH_4 or CO molecules and the reduction kinetics of active sites at the solid surfaces. They condition the initiating period of oxidation reaction (ranging between 10 and 20 minutes in the present experiments). It should be interesting to note that the K_1 parameter can be used to interpret the experimental undulations of the intensity I^*, just before this intensity reaches a constant value. Both K_0 and K_1 parameters might be directly linked to the presence or not of adsorbed species on the surfaces of polycrystalline solids. The K_2 parameter plays a moderate role in fitting calculated curves to experimental data.

Acknowledgments

The authors gratefully acknowledge the Provence-Alpes-Côte d'Azur Regional Council, the General Council of Var, and the agglomeration community of Toulon Provence Mediterranean for their helpful financial supports. This work was developed in the general framework of ARCUS CERES project (2008–2011).

References

[1] L. Bourja, B. Bakiz, A. Benlhachemi et al., "Structural, microstructural and surface properties of a specific CeO_2-Bi_2O_3 multiphase system obtained at 600∘C," *Journal of Solid State Chemistry*, vol. 184, no. 3, pp. 608–614, 2011.

[2] X. Zheng, X. Zhang, Z. Fang, X. Wang, S. Wang, and S. Wu, "Characterization and catalysis studies of CuO/CeO_2 model catalysts," *Catalysis Communications*, vol. 7, no. 9, pp. 701–704, 2006.

[3] J. Kašpar and P. Fornasiero, "Nanostructured materials for advanced automotive de-pollution catalysts," *Journal of Solid State Chemistry*, vol. 171, no. 1-2, pp. 19–29, 2003.

[4] R. Di Monte and J. Kašpar, "On the role of oxygen storage in three-way catalysis," *Topics in Catalysis*, vol. 28, no. 1–4, pp. 47–58, 2004.

[5] A. C. Ferreira, A. M. Ferraria, A. M. B. do Rego et al., "Partial oxidation of methane over bimetallic copper-cerium oxide catalysts," *Journal of Molecular Catalysis A*, vol. 320, no. 1-2, pp. 47–55, 2010.

[6] E. Aneggi, M. Boaro, C. De Leitenburg, G. Dolcetti, and A. Trovarelli, "Insights into the redox properties of ceria-based oxides and their implications in catalysis," *Journal of Alloys and Compounds*, vol. 408-412, pp. 1096–1102, 2006.

[7] M. Mogensen, N. M. Sammes, and G. A. Tompsett, "Physical, chemical and electrochemical properties of pure and doped ceria," *Solid State Ionics*, vol. 129, no. 1, pp. 63–94, 2000.

[8] R. N. Blumenthal and R. K. Sharma, "Electronic conductivity in nonstoichiometric cerium dioxide," *Journal of Solid State Chemistry*, vol. 13, no. 4, pp. 360–364, 1975.

[9] X. Zhang, A. B. Walters, and M. A. Vannice, "NOx decomposition and reduction by methane over La2O3," *Applied Catalysis B*, vol. 4, no. 2-3, pp. 237–256, 1994.

[10] K. Sato, J. Nakamura, T. Uchijima et al., "Role of rhodium anode in the YSZ-aided CH4 oxidation into syngas," *Solid State Ionics*, vol. 136-137, pp. 753–759, 2000.

[11] G. Jia, C. Zhang, L. Wang, S. Ding, and H. You, "Preparation and luminescence properties of lutetium oxide hollow spheres by a template-directed route," *Journal of Alloys and Compounds*, vol. 509, no. 22, pp. 6418–6422, 2011.

[12] X. J. Liu, H. L. Li, R. J. Xie, N. Hirosaki, X. Xu, and L. P. Huang, "Synthesis, characterization, and luminescent properties of Lu2O3:Eu phosphors," *Journal of Luminescence*, vol. 127, no. 2, pp. 469–473, 2007.

[13] E. Zych, "Luminescence and scintillation of inorganic phosphor materials," in *Handbook of Luminescence, Display Materials and Devices*, H. S. Nalwa and L. S. Rohwer, Eds., vol. 2, American Scientific Publishers, Valencia, Calif, USA, 2003.

[14] A. García-Murillo, C. Le Luyer, C. Dujardin et al., "Elaboration and scintillation properties of Eu^{3+}-doped Gd_2O_3 and Lu_2O_3 sol-gel films," *Nuclear Instruments and Methods in Physics Research A*, vol. 486, no. 1-2, pp. 181–185, 2002.

[15] T. Hattori, J. I. Inoko, and Y. Murakami, "Catalytic activity of lanthanide oxides in oxidation of butane," *Journal of Catalysis*, vol. 42, no. 1, pp. 60–72, 1976.

[16] M. Avrami, "Kinetics of phase change. I: general theory," *The Journal of Chemical Physics*, vol. 7, no. 12, pp. 1103–1112, 1939.

[17] M. Avrami, "Kinetics of phase change. II Transformation-time relations for random distribution of nuclei," *The Journal of Chemical Physics*, vol. 8, no. 2, pp. 212–224, 1940.

[18] M. Avrami, "Granulation, phase change, and microstructure kinetics of phase change. III," *The Journal of Chemical Physics*, vol. 9, no. 2, pp. 177–184, 1941.

[19] B. Bakiz, F. Guinneton, J. P. Dallas, S. Villain, and J. R. Gavarri, "From cerium oxycarbonate to nanostructured ceria: relations between synthesis, thermal process and morphologies," *Journal of Crystal Growth*, vol. 310, no. 12, pp. 3055–3061, 2008.

[20] B. Bakiz, F. Guinneton, M. Arab, S. Villain, A. Benlhachemi, and J. R. Gavarri, "Temperature dependent electrical properties and catalytic activities of La_2O_3–CO_2–H_2O Phase System," *Advances in Materials Science and Engineering*, vol. 2009, Article ID 612130, 4 pages, 2009.

[21] B. Bakiz, F. Guinneton, M. Arab et al., "Carbonatation and decarbonatation kinetics in the La_2O_3–$La_2O_2CO_3$ system under CO_2 gas flows," *Advances in Materials Science and Engineering*, vol. 2010, Article ID 360597, 6 pages, 2010.

[22] J. R. Gavarri, L. Bourja, B. Bakiz et al., "Structural and raman vibrational studies of CeO_2-Bi_2O_3 oxide system," *Advances in Materials Science and Engineering*, vol. 2009, Article ID 502437, 4 pages, 2009.

[23] S. Brunauer, P. H. Emmett, and E. Teller, "Adsorption of gases in multimolecular layers," *Journal of the American Chemical Society*, vol. 60, no. 2, pp. 309–319, 1938.

[24] P. Nowakowski, S. Villain, A. Kopia, I. Suliga, and J. R. Gavarri, "Catalytic conversion of air-methane flow by nanostructured ruthenium dioxide: FTIR spectroscopy and modeling," *Applied Surface Science*, vol. 254, no. 18, pp. 5675–5682, 2008.